



Mahmoudi, Ghodrat and Bauza, Antonio and Frontera, Antonio and Garczarek, Piotr and Stilinović, Vladimir and Kirillov, Alexander M. and Kennedy, Alan and Ruiz-Pérez, Catalina (2016) Metal-organic and supramolecular lead(II) networks assembled from isomeric nicotinoylhydrazone blocks : the effects of ligand geometry and counterion on topology and supramolecular assembly. CrystEngComm, 18 (28). pp. 5375-5385. ISSN 1466-8033 , <http://dx.doi.org/10.1039/C6CE00900J>

This version is available at <https://strathprints.strath.ac.uk/56568/>

Strathprints is designed to allow users to access the research output of the University of Strathclyde. Unless otherwise explicitly stated on the manuscript, Copyright © and Moral Rights for the papers on this site are retained by the individual authors and/or other copyright owners. Please check the manuscript for details of any other licences that may have been applied. You may not engage in further distribution of the material for any profitmaking activities or any commercial gain. You may freely distribute both the url (<https://strathprints.strath.ac.uk/>) and the content of this paper for research or private study, educational, or not-for-profit purposes without prior permission or charge.

Any correspondence concerning this service should be sent to the Strathprints administrator: strathprints@strath.ac.uk



Journal Name

ARTICLE

Metal-organic and Supramolecular Lead(II) Networks Assembled from Isomeric Nicotinoylhydrazone Blocks: The Effects of Ligand Geometry and Counter-ion on Topology and Supramolecular Assembly

Received 00th January 20xx,
Accepted 00th January 20xx

DOI: 10.1039/x0xx00000x

www.rsc.org/

Ghodrat Mahmoudi,^{a*} Antonio Bauzá,^b Antonio Frontera,^b Piotr Garczarek,^cVladimir Stilinović,^{d*} Alexander M. Kirillov,^{e*} Alan Kennedy^f and Catalina Ruiz-Pérez^g

A new series of six structurally diverse lead(II) coordination compounds was assembled from two isomeric nicotinoylhydrazones as neutral ligands and three Pb(II) salts with different monoanions (chloride, nitrate and thiocyanate) as starting materials. The products were isolated in good yields and were fully characterized, including by single-crystal X-ray diffraction and theoretical methods. Within the six compounds, three feature 2D metal-organic networks, two are 1D coordination polymers, and another one comprises discrete 0D dimeric units. The structures of the latter low dimensional compounds are extendable into 2D supramolecular networks. The topology of the coordination or supramolecular networks is primarily dictated by the geometry of the nicotinoylhydrazone used as a main building block. In contrast, supramolecular interactions are greatly influenced by the choice of the anion in the starting lead(II) salt, which is demonstrated by Hirshfeld surface analysis. In fact, the topological analysis and classification of metal-organic or supramolecular underlying networks in the obtained compounds was performed, disclosing the **hcb**, **2C1**, **gek1**, **SP 1-periodic net** (4,4)(0,2) and **3,4L83** topological types; the latter topology was documented for three compounds, including both coordination and supramolecular networks. In two compounds containing thiocyanate moieties there are supramolecular contacts between thiocyanate anions and lead centres. These were shown by DFT calculations to be strong tetrel bonds (−15.3 and −16.7 kcal/mol) between the σ -hole of the lead atom and the π -system of the thiocyanate S–C bond.

1. Introduction

The research on metal-organic frameworks (MOFs) or coordination polymers (CPs) is nowadays among the most attractive areas in modern chemistry.^{1–11} This is largely due to promising and already recognized applications of such

compounds as functional materials in gas storage and separation,^{12–17} catalysis,^{18–21} chemical sensing^{22–24} and many other areas. Therefore, substantial effort has been put into the design and synthesis of novel MOFs or CPs with a multitude of different structural and topological types, since the combination of metal nodes and organic spacers or linkers provides unlimited possibilities for the fabrication of materials with various structures and functions.

The structures and properties of CPs depend on a number of factors such as, for example, (1) the coordination geometries of metal centres, (2) the geometries and connectivity of ligands, (3) the supramolecular interactions between the CPs' components and (4) the presence of neighbouring/interpenetrating nets or interstitial guest molecules. If the organic ligands are neutral molecules, CPs would typically include inorganic ions which will either occupy interstices in the structures or act as additional ligands.^{25–31} Because of this, the choice of counter-ions can play a significant role in guiding the structures of MOFs or CPs that are driven by organic building blocks.^{32–37}

The metal-organic networks or coordination polymers based on lead(II) remain less explored, mostly due to the toxicity of this metal, as well as its somewhat unpredictable coordination behaviour. In fact, the electronic configuration of Pb(II) allows

^a Young Researchers and Elite Club, Tabriz Branch, Islamic Azad University, Tabriz, Iran. E-mail: mahmoudi_ghodrat@yahoo.co.uk

^b Department of Chemistry, Universitat de les Illes Balears, Crta. de Valldemossa Km 7,5, 07122 Palma de Mallorca (Balears), Spain. E-mail: toni.frontera@uib.es

^c Faculty of Chemistry, Wrocław University of Technology, 27 Wybrzeże Wyspiańskiego Street, 50-370 Wrocław, Poland

^d Department of Chemistry, Faculty of Science, University of Zagreb, Horvatovac 102a, HR-10000 Zagreb, Croatia.

^e Centro de Química Estrutural, Complexo I, Instituto Superior Técnico, Universidade de Lisboa, Av. Rovisco Pais, 1049-001, Lisbon, Portugal, E-mail: kirillov@tecnico.ulisboa.pt

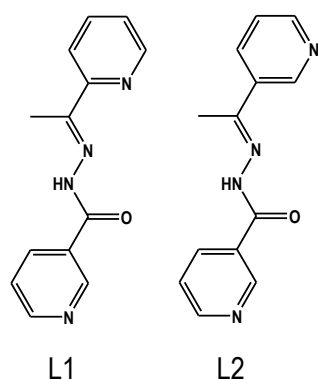
^f Department of Pure & Applied Chemistry, University of Strathclyde, 295 Cathedral Street, Glasgow G1 1XL, Scotland, UK

^g Laboratorio de Rayos X y Materiales Moleculares, Dpto. Física Fundamental II, Facultad de Física, Universidad de La Laguna, E-38204 La Laguna, Tenerife, Spain.

Electronic Supplementary Information (ESI) available: CCDC 1474988–1474993 contain the supplementary crystallographic data for 1–6. These data can be obtained free of charge via <http://www.ccdc.cam.ac.uk/conts/retrieving.html>, or from the Cambridge Crystallographic Data Centre, 12, Union Road, Cambridge CB2 1EZ, UK; Fax: (+44) 1223-336-033; or e-mail: deposit@ccdc.cam.ac.uk.

the Pb^{2+} cation to exhibit a large variety of coordination numbers (from 2 to 10) and geometries. However, the interest in CPs of lead has recently substantially increased. This is presumably related to the diversity of coordination modes of this metal and the unique supramolecular architectures and physical properties of such compounds.³⁸⁻⁴⁶ Hence, the Pb-based CPs find potential applications as luminescent materials,⁴⁷⁻⁵² ion exchangers⁵³ and nonlinear optical materials.⁵⁴ As Pb(II) cations have an affinity towards organic ligands containing O, N and S donor atoms,⁵⁵⁻⁵⁹ hydrazone containing building blocks are often employed in construction of Pb(II) coordination compounds, also due to their excellent coordinating ability, versatile coordination modes, and possible supramolecular interactions.

An additional interest in the chemistry of Pb(II) arises from our recent work and concerns the unique ability of lead(II) to participate in the formation of tetrel bonds.⁶⁰ This newly (re)discovered supramolecular interaction⁶¹⁻⁶⁶ is formed between a positively charged region on a group 14 atom in continuation of a covalent bond (a σ -hole) and an electron donor, analogously to a more common halogen bond. Lead(II) is particularly prone to the formation of tetrel bonds because of its size and polarizability, as well as its specific hemidirectional coordination^{67,68} which leaves a gap in the coordination sphere of the Pb(II) cation, thus enabling the approach of the electron-donor. This makes lead(II) metal-organic networks particularly sensitive to the choice of ligands and counter-ions to form supramolecular interactions not only between each other, but also with the metal ion itself.



Scheme 1. Molecular diagrams of nicotinoylhydrazone building blocks L1 and L2.

Herein we describe a study of the effect of counter-ion on the topology, geometry, and supramolecular structure of metal-organic frameworks in two series of coordination compounds having a general formula $[\text{PbLX}_2]$, where X is a singly charged anion (Cl^- , NO_3^- , or SCN^-), and L is a nicotinoylhydrazone ligand. The effect of the counter-ion was tested against two isomeric ligands L1 and L2, differing only in the position of pyridyl nitrogen atom within one of the pyridine rings (Scheme 1). This difference renders their potential for assembling rather distinct metal-organic frameworks, as L1 is expected to act as bridging block between two metal centres (chelating mode and binding via a pyridine nitrogen atom), while L2 can bridge three metal

centres (binding *via* the central hydrazone group and two interactions involving two terminal pyridine nitrogen atoms). On the other hand, the counter-ions widely differ in their coordination ability, as well as in the possibility for the formation of supramolecular interactions, in particularly hydrogen and tetrel bonds. These factors can thus exert a decisive control over the structure of the resulting solids.

2. Experimental

2.1. Materials and measurements

The nicotinoylhydrazone derivatives (L1 and L2) were prepared following the reported method⁴⁰ and used without further purification. All other reagents and solvents used for the synthesis and analysis were commercially available and were used as received. FT-IR spectra were recorded on a Bruker Tensor 27 spectrometer. Microanalyses were performed using a Heraeus CHN-O-Rapid analyser. Syntheses were carried out using a branched tube apparatus.

2.2. Syntheses of lead(II) compounds (1-6)

[Pb(L1)Cl₂]_n (1) Lead(II) chloride (0.027 g, 0.1 mmol), and L1 (0.024 g, 0.1 mmol) were combined in the main arm of a branched tube. Methanol (10 ml) was carefully added to fill the arms. The tube was sealed and immersed in an oil bath at 60 °C, while the branched arm was kept at ambient temperature. After one day, crystals of **1** formed in the cooler arm, and were filtered off, washed with acetone and ether, and then dried in air. The isolated yield was 68%. Anal. calcd. (found) for $\text{C}_{13}\text{H}_{12}\text{Cl}_2\text{PbN}_4\text{O}$: C, 30.12 (30.22); H, 2.33 (2.37); N, 10.81 (10.67) %. IR (cm^{-1}) selected bands: 546(w), 662(vs), 786(vs), 941(m), 1067 (w), 1133(m), 1204(s), 1284(s), 1422(s), 1469(s), 1587(s), 1640(s), 3089(w).

[Pb(L1)(NO₃)₂]_n (2) Similarly to **1**, equimolar amounts of $\text{Pb}(\text{NO}_3)_2$ and L1 were used in the same branched tube apparatus under the same conditions. For **2**, the isolated yield was 74%. Anal. calcd. (found) for $\text{C}_{13}\text{H}_{12}\text{PbN}_6\text{O}_7$: C, 27.32 (27.25); H, 2.12 (2.10); N, 14.71 (14.77) %. IR (cm^{-1}) selected bands: 474(w), 625(m), 821(vs), 897 (m), 1013(s), 1280(m), 1351(s), 1382(s), 1442(s), 1528(vs), 1589(m), 1634(m), 3073(w).

[Pb(L1)(SCN)₂]₂ (3) Similarly to **1** and **2**, equimolar amounts of $\text{Pb}(\text{SCN})_2$ and L1 were reacted in the same branched tube apparatus, under the identical conditions. For **3**, the isolated yield was 70%. Anal. calcd. (found) for $\text{C}_{30}\text{H}_{24}\text{Pb}_2\text{N}_{12}\text{O}_2\text{S}_4$: C, 31.97 (32.02); H, 2.15 (2.17); N, 14.91 (14.87) %. IR (cm^{-1}) selected bands: 527(w), 690(s), 776(m), 1058 (w), 1156(m), 1256(w), 1439(m), 1592(m), 1623(s), 3060(w).

[Pb(L2)Cl₂] (4) For **4**, a similar synthetic procedure to **1** was utilized, except that L1 was replaced by L2. The isolated yield was 78%. Anal. calcd. (found) for $\text{C}_{13}\text{H}_{12}\text{Cl}_2\text{PbN}_4\text{O}$: C, 30.12 (30.26); H, 2.33 (2.30); N, 10.81 (10.77) %. IR (cm^{-1}) selected bands: 574(w), 694(s), 780(s), 1003 (w), 1159(m), 1250(w), 1437(m), 1576(s), 1612(s), 3060(w).

[Pb(L2)(NO₃)₂]_n (5) For **5**, the synthesis was the same as for **2**, but using L2 instead of L1. The isolated yield was 88%. Anal. calcd. (found) $\text{C}_{13}\text{H}_{12}\text{PbN}_6\text{O}_7$: C, 27.32 (27.22); H, 2.12 (2.17); N, 14.71 (14.67) %. IR (cm^{-1}) selected bands: 625(m), 813(vs), 900

(m), 1027(s), 1195(m), 1312(s), 1381(s), 1536(s), 1595(vs), 1629(m), 3057(w).

[Pb(L2)(SCN)₂]_n (6) For **6**, the synthesis was the same as for **3**, but using L2 instead of L1. The isolated yield was 90%. Anal. calcd. (found) for C₁₃H₁₂PbN₆OS: C, 31.97 (32.09); H, 2.15 (2.20); N, 14.91 (14.97) %. IR (cm⁻¹) selected bands: 541(w), 696(s), 810(m), 1027 (w), 1196(m), 1294(w), 1473(m), 1624(m), 2061(s), 2926(w)

2.3. X-ray crystallography

Single crystals of **1-6** suitable for X-ray analyses were selected and crystallographic data were collected on Enraf Nonius FR590 or Oxford Diffraction Xcalibur E⁶⁸ or Bruker-AXS Kappa APEX II CCD^{69,70} diffractometers using Mo K_α radiation (λ = 0.71073 Å). Each data set was treated with SADABS absorption corrections based on redundant multi-scan data.⁷¹ All the structures were solved by direct methods and refined by full matrix least-squares procedures.⁷² All non-hydrogen atoms were refined with anisotropic displacement parameters whereas hydrogen atoms not involved in hydrogen bonding were placed in calculated positions and given isotropic *U* values 1.2 times that of the atom to which they are bonded.

2.4. Topological analysis

Topological analysis of coordination (or supramolecular) networks in **1-6** was performed using Topos software and following the concept of the simplified underlying net.^{73,74} Such nets were generated by contracting organic ligands (for analysis of coordination polymers) or discrete metal-complex units (for analysis of supramolecular networks), maintaining their connectivity via coordination bonds (including some rather long bonds/interactions) or hydrogen bonds. For the analysis of networks involving H-bonding interactions, only strong D–H...A hydrogen bonds were considered, wherein the H...A < 2.50 Å, D...A < 3.50 Å, and ∠(D–H...A) > 120°; D and A stand for donor and acceptor atoms.⁷³

2.5. Theoretical methods

The geometries of the compounds included in this study were computed at the BP86-D3/def2-TZVP level of theory using the crystallographic coordinates within the TURBOMOLE program.⁷⁵ This level of theory that includes the latest available dispersion correction (D3) is adequate for studying non covalent interactions dominated by dispersion effects like π-stacking. The basis set superposition error for the calculation of interaction energies has been corrected using the counterpoise method.⁷⁶ The “atoms-in-molecules” (AIM)⁷⁷ analysis of the electron density has been performed at the same level of theory using the AIMAll program.⁷⁸

2.6. Hirshfeld surface analysis

Hirshfeld surfaces⁷⁹⁻⁸¹ and fingerprint plot (*d_e* vs. *d_i*) calculations were performed using the Crystal Explorer package ver. 3.1.⁸² Crystal structures were imported from CIF files. Hirshfeld surfaces were generated for complex molecules using high resolution and mapped with the *d_{norm}* or shape index functions.

3. Results and discussion

3.1. Synthesis and spectroscopic results

The reactions of L1 or L2 with PbX₂ (X = Cl, NO₃ and SCN), in a 1:1 molar ratio in methanol, resulted in the formation of compounds **1-6**. In the IR spectra of **1-6**, the ν(C=N) + ν(C=C) stretching vibrations³¹ are in the 1650-1560 cm⁻¹ range, being characteristic for hydrazones bound to a metal ion. The bands at 1317, 1031 and 849 cm⁻¹ are assignable to ν_{as}(NO₃), ν_s(NO₃) and δ(NO₃) vibrations of nitrate ligands in **2**, but in **5** these bands appear at 1312, 1027 and 813 cm⁻¹. The separation between the ν_{as} and ν_s bands corroborates the symmetric coordination of the nitrate ion.²² In **4**, the ν_{as}(NCS) and ν(CS) stretches of S-coordinated thiocyanate²¹ appear as strong bands at 2111 and 765 cm⁻¹, respectively. Additionally, a δ(NCS) band is found at 452 cm⁻¹. All other less characteristic vibrations of organic ligands are seen in the 1600-600 cm⁻¹ range (Table 2; Fig. S1).

3.2. Crystal structures of 1-6

Complex **1** crystallizes in *P*2₁/*c* space group. The asymmetric unit consists of one lead(II) atom, one μ₂-L1 tetradentate ligand and two chloride moieties (one terminal and μ₂-bridging). The Pb1 centres adopt a distorted pentagonal bipyramid geometry with three chelating atoms from one L1 moiety, pyridyl nitrogen from a second L1 molecule and a terminal chloride ligand in the equatorial positions. The axial sites are taken by two symmetry equivalent μ₂-Cl ligands. The Pb–N and Pb–Cl bond distances are in the 2.640(2)–2.841(2) and 2.7027(8)–3.1048(8) Å range, respectively. The Pb–O bond has a length of 2.586(2) Å. The 3-pyridyl groups of the L1 ligands bind adjacent Pb1 atoms forming centrosymmetric dimeric units, whereas the μ₂-Cl linkers bridge these dimeric units generating a 2D metal-organic network perpendicular to the crystallographic axis *a* (Figure 1a). For the sake of topological analysis, this network was simplified^{73,74} resulting in a uninodal 3-connected underlying net (Figure 1b). It is composed of the 3-connected Pb1 nodes and the 2-connected μ₂-L1 and μ₂-L1 linkers, and displays the **hcb** [Shubnikov hexagonal plane net/(6,3)] topology with the point symbol of (6³). Besides, the terminal chloride ligand acts as an acceptor in N–H...Cl (N3–H3...Cl1 of 3.285 Å) hydrogen bonds and weak C–H...Cl contacts (C7–H7C...Cl1 and C11–H11...Cl2), thus resulting in the extension of 2D metal-organic layers into a 3D supramolecular structure.

Compound **2** crystallizes in *P* $\bar{1}$ space group with one lead(II) atom, one L1 moiety and two nitrate ligands (one terminal and one μ₂-bridging) in the asymmetric unit. The Pb1 atom is bound by a tridentate chelating L1 moiety, as well as one terminal bidentate and two bridging μ₂-nitrate ligands. The latter bind adjacent Pb1 centres to form centrosymmetric dimers. The Pb–O bond distances fall into the 2.511(2)–2.867(2) Å range, whereas the Pb–N distances vary from 2.531(2) to 2.638(2) Å. The eighth coordination position is occupied by a pyridyl nitrogen from a second L1 molecule, with an elongated Pb–N bond (2.923(2) Å). The resulting structure can be considered as a zigzag 1D metal-organic chain (Figure 2a). Topological analysis of this chain discloses a 2-connected underlying 1D network

with the **2C1** topology (Figure 2b). The adjacent chains are interconnected by hydrogen bonds between the N–H groups of L1 moieties and terminal nitrate ligands (N3–H3...O2 of 2.971 Å forming a centrosymmetric $R_2^2(12)$ motif) into 2D H-bonded layers perpendicular to the *a* axis. There is also a π - π stacking between the L1 ligands in adjacent chains (closest contact, C3...C11 of 3.318 Å, is between 2-pyridyl and 3-pyridyl carbon atoms).

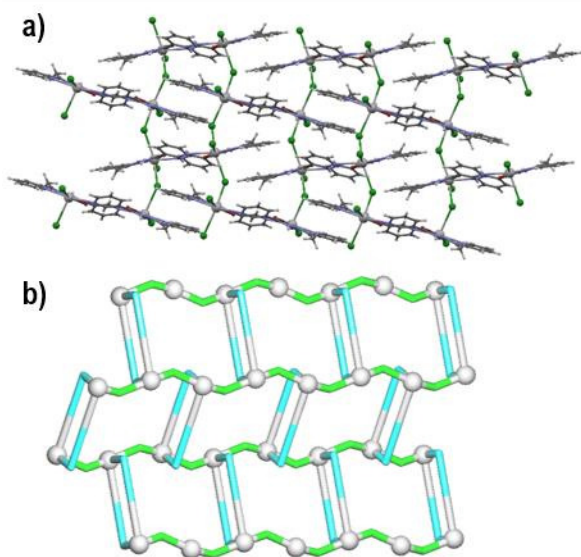


Figure 1. Structural fragments of **1** viewed along the *a* axis. (a) 2D metal-organic network. (b) Topological representation of a simplified underlying network showing a uninodal 4-connected metal-organic layer with the **hcb** [Shubnikov hexagonal plane net/(6,3)] topology; colour codes: 4-connected Pb1 nodes (grey balls), centroids of 2-connected μ_2 -L1 (cyan) and μ_2 -Cl (green) linkers.

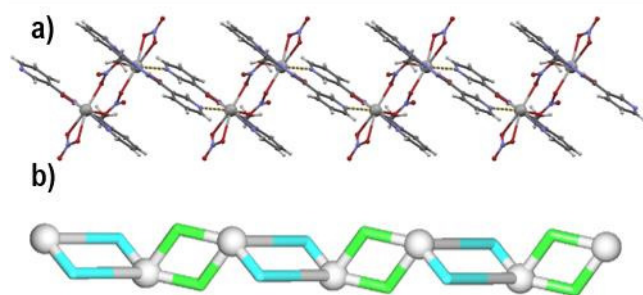


Figure 2. Structural fragments of **2** viewed along the *c* axis. (a) Binding of the $[\text{PbL1}(\text{NO}_3)_2]_2$ units into a zigzag 1D metal-organic chain (elongated Pb...N bonds are drawn as stippled lines). (b) Topological representation of a simplified underlying network showing a uninodal 2-connected chain with the **2C1** topology; colour codes: 2-connected Pb1 nodes (grey balls), centroids of 2-connected μ_2 -L1 (cyan) and μ_2 -Cl (green) linkers.

Although compound **3** also crystallizes in $P\bar{1}$ space group, its asymmetric unit consists of a non-centrosymmetric dimer comprising two crystallographically nonequivalent lead(II) atoms, two μ_2 -L1 moieties and four thiocyanate ligands (Figure

3a). Both six-coordinate lead(II) atoms are surrounded by the tridentate μ_2 -L1 ligands, pyridyl nitrogen of the other L1 moiety and two terminal N- and S-bound thiocyanates. However, a relative disposition of donor atoms around the two lead centres is markedly different. The Pb1 atom is coordinated in an extremely disordered octahedral fashion with the chelating and monodentate L1 moieties lying in one plane and the two thiocyanate ligands in *trans* position. The Pb2 centre adopts a distorted pentagonal pyramidal coordination environment with one oxygen and four nitrogen atoms (from two L1 moieties as well as one thiocyanate ligand) in the basal sites, whereas a thiocyanate S atom takes the apical position. The thiocyanate ligands bonded to Pb2 are thus at an angle of ca. 72°, as opposed to Pb1 where they are in a *trans* configuration (ca. 152°). Another significant difference is in the Pb–N bond lengths between the lead(II) centres and the pyridyl N atoms; it is normal for Pb2 (2.76 Å), but extremely long for Pb1 (3.20 Å). Other than this, the Pb–O, Pb–N, and Pb–S bond lengths are within normal ranges of 2.518(3)–2.525(3), 2.506(3)–2.763(3), and 2.8335(9)–3.0019(10) Å, respectively.

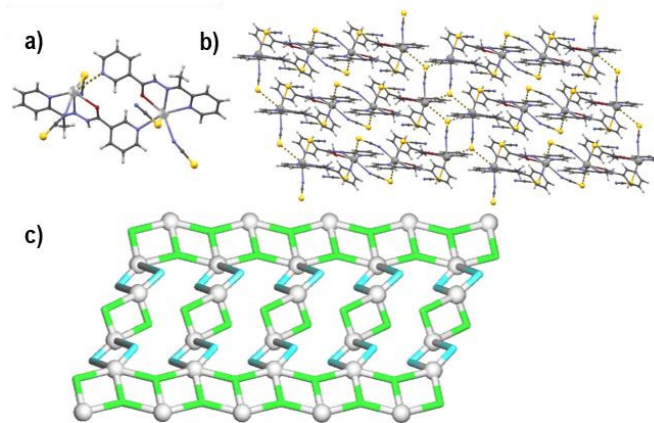


Figure 3. Structural fragments of **3**. (a) A non-centrosymmetric $[\text{PbL1}(\text{SCN})_2]_2$ dimeric unit (a) long intramolecular Pb...N contact is drawn as a stippled line. (b) Binding of $[\text{PbL1}(\text{SCN})_2]_2$ dimers into a supramolecular 2D sheet perpendicular to [101] direction (intermolecular Pb...S contacts are drawn as stippled lines). (c) Topological representation of a simplified underlying network showing a binodal 3,4-connected supramolecular layer with the **3,4L83** topology; colour codes: Pb1 nodes and Pb2 linkers (grey balls), centroids of L1 linkers (cyan), and centroids of SCN nodes and linkers (green); view along the *c* axis.

Interestingly, in spite of the differences in coordination environment, both lead atoms are hemidirectionally coordinated and are involved in supramolecular tetrel bonding with the sulphur atoms of the N-bound thiocyanate ligands of the neighbouring dimers. The Pb1 centre thus binds to two S4 atoms from two dimers, while the Pb2 centre binds to the S2 atom from a third dimer moiety. This leads to the formation of a supramolecular layer perpendicular to the [011] direction (Figure 3b). From a topological perspective,^{73,74} this supramolecular 2D layer can be classified as a binodal 3,4-connected underlying net with the **3,4L83** topology (Figure 3c). It is described by the point symbol of $(4^2.6^3.8)(4^2.6)$, wherein the

(4².6³.8) and (4².6) notations are those of the 4-connected Pb1 and the 3-connected thiocyanate nodes, respectively. There are also Pb2, L1 and other thiocyanate moieties that participate in the formation of the net and which are considered as linkers. Compound **4** crystallizes in $P\bar{1}$ space group and has a lead(II) atom, a μ_3 -L2 block, one μ_2 -bridging and one terminal chloride ligand in the asymmetric unit. Lead(II) centre is octahedrally coordinated by three Cl ligands as well as two pyridyl nitrogen atoms and a carbonyl oxygen atom from three L2 moieties. These in turn act as tridentate bridging ligands and coordinate three different Pb ions. The μ_2 -Cl and μ_3 -L2 moieties act as linkers and spacers and interconnect the adjacent Pb1 atoms to give a 2D metal-organic network (Figure 4a). The adjacent 2D sheets in **4** are further interconnected along the a axis by the N3-H3...Cl2 hydrogen bonds, involving the amide N-H group of L2 and the terminal chloride ligand. Topological classification of such 2D sheets discloses a binodal 3,4-connected underlying network with the **3,4L83** topology (Figure 4b). Although this topology is similar to that of supramolecular net **3**, it however corresponds to the metal-organic net in **4**.

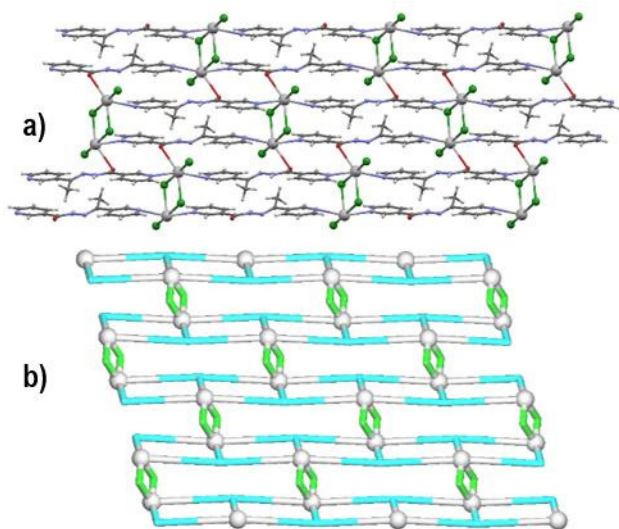


Figure 4. Structural fragments of **4** viewed along the a axis. (a) 2D metal-organic network. (b) Topological representation of a simplified underlying 2D network showing a binodal 3,4-connected metal-organic layer with the **3,4L83** topology; colour codes: 4-connected Pb1 nodes (grey balls), centroids of 3-connected μ_3 -L2 nodes (cyan), and centroids of 2-connected μ_2 -Cl linkers (green).

Compound **5** crystallizes in the $P2_1/c$ space group and possesses one lead(II) centre, one μ_3 -L2 block, and two nitrate ligands (one μ_2 -bridging and one terminal) in the asymmetric unit. Lead(II) centre is eight-coordinated by six oxygen atoms, coming from one L2 moiety and three nitrate ligands, and two nitrogen atoms from two different L2 blocks. Bond distances lay in the range of 2.551(2)–2.874(2) Å for Pb-O bonds and 2.722(3)–2.776(3) Å for Pb-N bonds. Similarly to **4**, each μ_3 -L2 moiety bridges three lead(II) atoms, whereas a μ_2 -nitrate ligand acts as an additional linker (Figure 5a). As a result, an intricate 2D metal-organic network is generated (Figure 5a). To get further insight into this rather complex network, we carried out its

topological analysis by generating a simplified underlying net. It is composed of the 5-connected Pb1 and the 3-connected μ_3 -L2 nodes, as well as the 2-connected μ_2 -nitrate linkers (Figure 5b). This net can be classified as a binodal 3,5-connected layer with a rare **gek1** topology. It is defined by the point symbol of (3.4.5)(3².4.5.6².7⁴), wherein the (3.4.5) and (3².4.5.6².7⁴) notations correspond to the μ_3 -L2 and Pb1 nodes, respectively. Besides, the adjacent metal-organic layers in **5** are extended into a 3D supramolecular network through weak C-H...O hydrogen bonds (C2-H2...O5, C10-H10...O4).

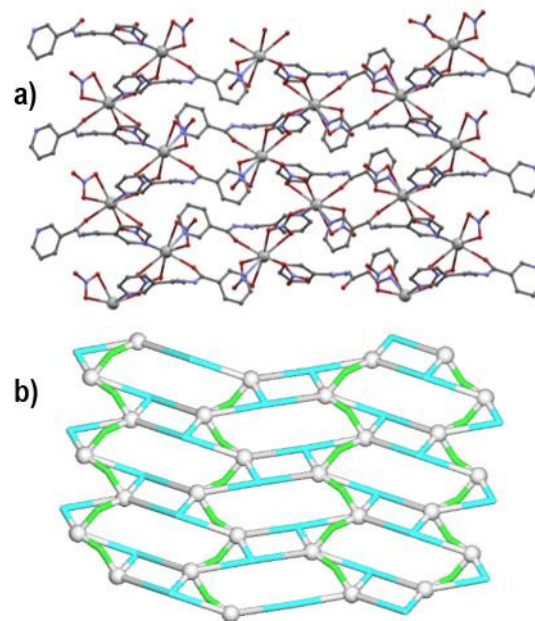


Figure 5. Structural fragments of **5** viewed along the a axis. (a) 2D metal-organic network (hydrogen atoms were omitted for clarity). (b) Topological representation of a simplified underlying 2D network showing a binodal 3,5-connected metal-organic layer with the **gek1** topology; colour codes: 5-connected Pb1 nodes (grey balls), centroids of 3-connected μ_3 -L2 nodes (cyan), and centroids of 2-connected μ_2 -NO₃ linkers (green).

Compound **6** crystallizes in $P\bar{1}$ space group and has one lead(II) atom, one μ_3 -L2 block, and two thiocyanate moieties (one terminal ligand and one anion) in the asymmetric unit (Figure 6). Lead(II) centre is four-coordinated showing a disphenoidal geometry that is filled by three μ_3 -L2 moieties (two *via* pyridine nitrogen and one *via* the oxygen atom), and a nitrogen atom from a thiocyanate ligand. Although the other thiocyanate is not coordinated to the Pb1 atom, it is hydrogen bonded to the amide N-H of L2 (N2-H2n...N6 of 2.939 Å). Each L2 bridges three lead(II) atoms, thus interconnecting them into a ladder like cationic [PbL2(SCN)]_nⁿ⁺ 1D chains along the [011] direction (Figure 6a). From a topological viewpoint,⁷³ these chains are driven by the 3-connected and topologically equivalent Pb1 and μ_3 -L2 nodes (Figure 6c). These chains can be classified as a uninodal 3-connected underlying net with the **SP 1-periodic net** (4,4)(0,2) topology and the point symbol of (4².6). The low coordination number of Pb1 allows an easy approach of two thiocyanate ions to the lead(II) centres, forming close Pb...S tetrel bonding contacts. These contacts interconnect the metal-

organic chains into supramolecular sheets perpendicular to the [101] direction (Figure 6b). Topological classification of such supramolecular sheets reveals the **3,4L83** topology, which is analogous to the coordination network in **4**.

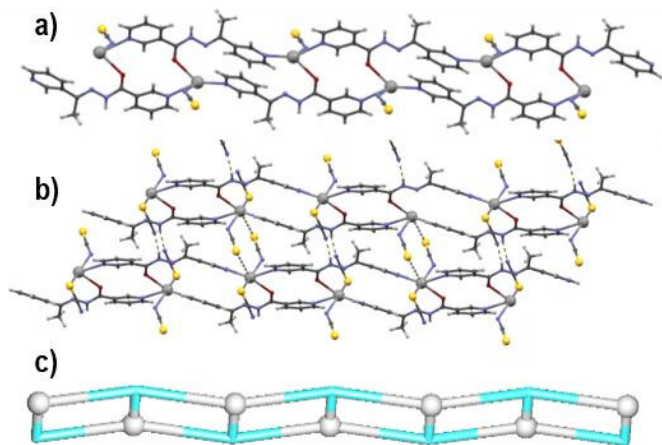


Figure 6. Structural fragments of **6**. (a) Cationic metal-organic $[\text{PbL}_2(\text{SCN})]_n^{n+}$ chain with H-bonded SCN^- anions. (b) Binding of $[\text{PbL}_2(\text{SCN})]_n^{n+}$ chains and SCN^- counter-ions into 2D sheets perpendicular to the [101] direction by supramolecular $\text{Pb}\cdots\text{S}$ and $\text{Pb}\cdots\text{C}$ interactions. (c) Topological representation of a simplified underlying 1D network showing a uninodal 3-connected metal-organic chain with the **SP 1-periodic net** (4,4)(0,2) topology; colour codes: 3-connected Pb1 nodes (grey balls), centroids of 3-connected $\mu_3\text{-L2}$ nodes (cyan); rotated view along the *a* axis.

3.3. Hirshfeld surface analysis

To analyse the intermolecular interactions in crystal structures of **1-6**, Hirshfeld surfaces have been calculated for all the structures. For polymeric structures (**1**, **2**, **4**, **5** and **6**) the Hirshfeld surfaces have been calculated around monomeric units. This leads to areas of the Hirshfeld surfaces with large d_{norm} values corresponding to coordination bonds (Figure 7).

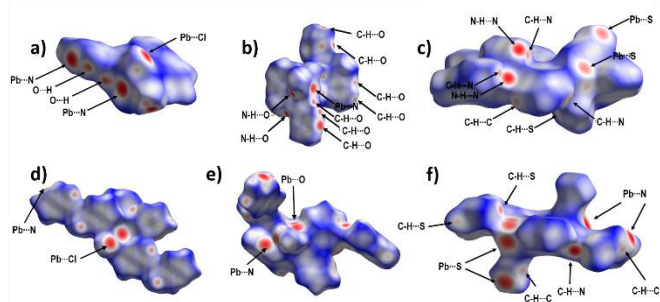


Figure 7. Hirshfeld surfaces mapped with d_{norm} for a) **1**, b) **2**, c) **3**, d) **4**, e) **5** and f) **6**.

The analyses of the Hirshfeld surfaces reveals that the dominant supramolecular interactions are primarily defined by the choice of the anionic co-ligand. Thus, in both **1** and **4** the dominant supramolecular interactions are hydrogen bonds involving the chloride ligands (24.6% of the Hirshfeld surface in **1** and 27.0% in **4**), and dispersive $\text{H}\cdots\text{H}$ contacts (24.0% of the Hirshfeld

surface in **1** and 26.1% in **4**). Of these most notable are numerous $\text{C-H}\cdots\text{Cl}$ and $\text{N-H}\cdots\text{Cl}$ hydrogen bonding contacts corresponding to areas of large values of d_{norm} (Figure 7 a and d). The most significant difference between **1** and **4** is in the importance of $\text{C-H}\cdots\pi$ interactions ($\text{H}\cdots\text{C}$ contacts comprising 21.0% of the HS in **1** but only 7.0% in **4**). This difference is readily observed when shape index function is mapped onto the Hirshfeld surfaces, as this clearly shows large red 'hollows' indicating presence of $\text{C-H}\cdots\pi$ interactions (marked with plain arrows on Fig. 8a) on the HS of **1** – a feature absent on the Hirshfeld surface of **4** (Fig. 8d).

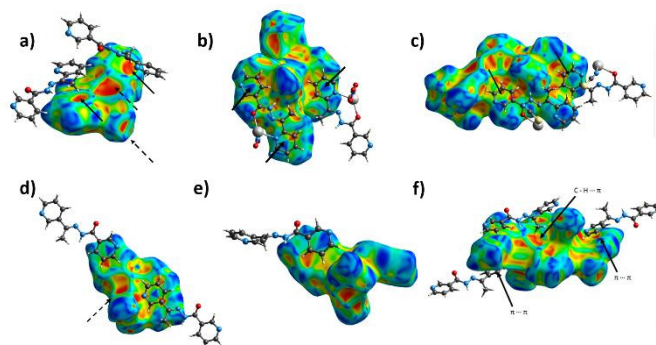


Figure 8. Hirshfeld surfaces mapped with shape index function for a) **1**, b) **2**, c) **3**, d) **4**, e) **5** and f) **6**. Dashed arrows denote parts of the surface corresponding to covalent bonds in polymeric compounds. Full arrows mark π stacking interactions, unless stated differently.

In **2** and **5** by far the most dominant feature are the $\text{O}\cdots\text{H}$ contacts (corresponding to 47.6% of the Hirshfeld surface in **2** and 41.1% in **5**) indicative of the numerous hydrogen bonds with nitrate oxygen atoms as acceptors. In both cases there is an area of large d_{norm} corresponding to the $\text{N-H}\cdots\text{O}$ hydrogen bond, and further numerous corresponding to $\text{C-H}\cdots\text{O}$ contacts. In addition, there are significant contributions of $\text{C-H}\cdots\pi$ interactions (11.2% in **2** and 11.4% in **5**) and dispersive $\text{H}\cdots\text{H}$ contacts (11.2% of the Hirshfeld surface in **2** and 18.7% in **5**). When shape index function is used to map the surface, bow-tie motifs can be noticed which indicate presence of aromatic ring stacking contacts (Fig. 8b and f).

The dominant supramolecular interactions in **3** and **6** are hydrogen bonding contacts, in particularly multiple strong $\text{N-H}\cdots\text{N}$ and weaker $\text{C-H}\cdots\text{N}$, $\text{C-H}\cdots\text{S}$, and $\text{C-H}\cdots\pi$ hydrogen bonds – $\text{N-H}\cdots\text{N}$ and $\text{C-H}\cdots\text{N}$ contacts constitute 18.0% of Hirshfeld surface in **3** and 13.2% in **6**, $\text{C-H}\cdots\text{S}$ hydrogen bonds 19.1% and 20.0%, and $\text{H}\cdots\text{C}$ contacts 19.7% and 19.9% respectively. Short $\text{N-H}\cdots\text{N}$ hydrogen bonds are noticeable as long, sharp 'spikes' on the 2D plot (Figure 9).

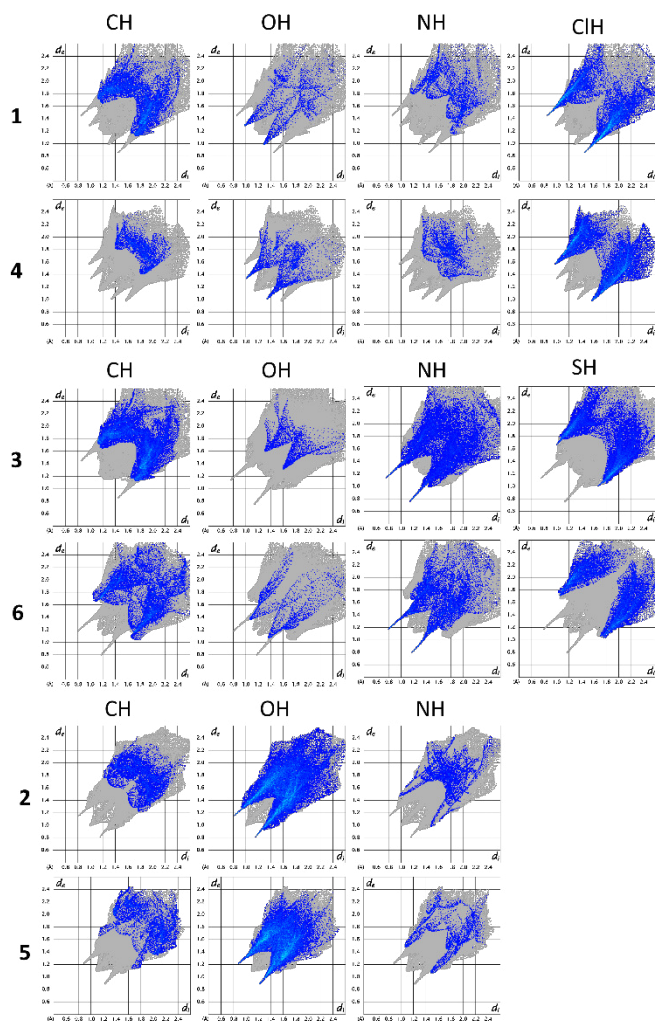


Figure 9. Decomposed fingerprint plots showing the main types of intermolecular contacts in structures of **1-6**.

A particularly interesting feature of structures **3** and **6** is the presence of Pb...S tetrel bonds. In order to observe them by Hirshfeld surface analysis it was necessary to define the unit of the polymeric **6** for which the Hirshfeld surface had to be expanded to include the two additional L2 ligands covalently bonded to the Pb centre, and contacts between the Pb centre within the surface and atoms outside were studied. In both **3** and **6** there are areas of high d_{norm} (Figure 10) corresponding to tetrel bonds between the Pb centre and thiocyanate ions. Interestingly, not only the thiocyanate sulphur, but also the carbon atom appears to be in contact with the lead(II) ions. This is apparent from the Hirshfeld surface mapped with d_{norm} as pairs of fused red circles, corresponding to pairs of Pb...S and Pb...C contacts. The corresponding traces in the decomposed fingerprint plots (Figure 11) are considerably different, with the trace corresponding to the Pb...S contact markedly sharper and Pb...C more diffuse. There is also in both structures a minute contribution of the Pb...N contact.

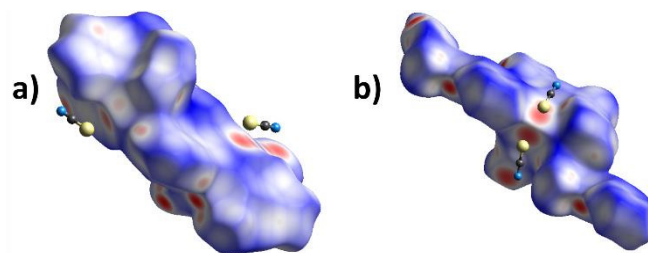


Figure 10. Hirshfeld surfaces mapped with d_{norm} for a) a molecule of **3** and b) an extended monomer of **6** showing the tetrel bonding between the Pb atoms (within the surface) and thiocyanate anions

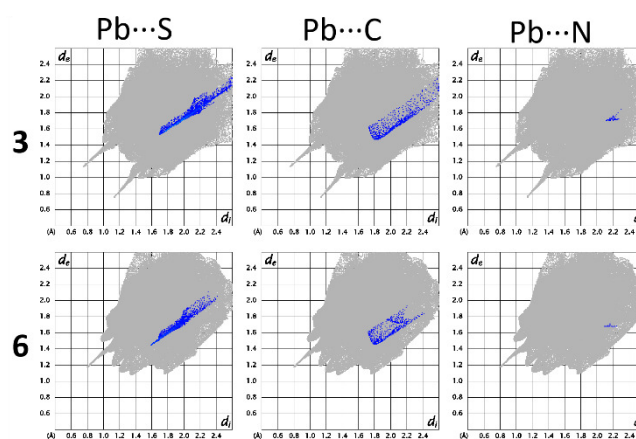


Figure 11 Decomposed fingerprint plots showing contacts including Pb in **3** and **6**.

3.4. DFT study

We have focused our study to the analysis of the noncovalent tetrel bonding interactions involving the Pb and several electron rich atoms. These interactions are very important governing the crystal packing, as has been explained above. Obviously in all structures reported herein, hydrogen bonding interactions are very relevant in the solid state, as demonstrated by the examination of the forces that govern the crystal packing and the Hirshfeld analysis (*vide supra*). However, in some structures (compounds **3** and **6**), the existence of noncovalent S...Pb noncovalent interactions is worth of investigation. Moreover, in compound **3** antiparallel stacking interactions between the pyridine rings of the organic ligands have been also investigated. We have first examined the molecular electrostatic potential surface (MEPS) of the asymmetric unit of compound **3** and a model of compound **6**, since it is polymeric. From the inspection of the surfaces, some considerations arise. First, small regions of positive potential (σ -holes) are clearly observed in the Pb atoms (+45 kcal/mol for **1** and +54 kcal/mol for **6**, see Figure 12) that anticipate their ability to interact with concentrations of negative charge. Second, the SCN co-ligands show ambidentate behaviour. That is, one is coordinated through the N-atom and the other through the S-atom. The electrostatic potential at the end of the ligand is very different depending on the type of coordination. The N-coordinated ligand presents a modest potential in the S end (−16 kcal/mol)

and, conversely, the S-coordinated ligand shows a strong electrostatic potential at the N end (-58 kcal/mol). This very different electrostatic characteristic of the SCN ligand is important in the crystal packing since the N-end of the Pb-SCN ligand in **3** interacts with the N-H group forming a strong H-bond as demonstrated in its Hirshfeld analysis (Figures 7 and 9).

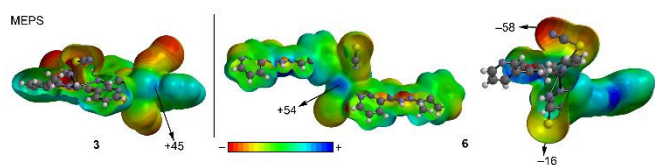


Figure 12. MEPS of compounds **3** and **6** at the B3LYP/6-31+G* level of theory.

At this point, it should be emphasized that the simultaneous ambidentate SCN coordination in Pb complexes is quite unusual. A search in the Cambridge Structural Database of complexes containing the $\text{Pb}(\text{SCN})_2$ fragment reveals that only three structures have been structurally characterized exhibiting both binding modes in the same complex ($\mu_{1,3}$ bridging ligands have not been considered in the search). Therefore, the complexes reported herein are exceptional in this sense. Interestingly, the CSD search also reveals that only 5 structures present both SCN co-ligands coordinated *via* the S atoms and that the usual behaviour is the coordination *via* the N atom (17 structures).

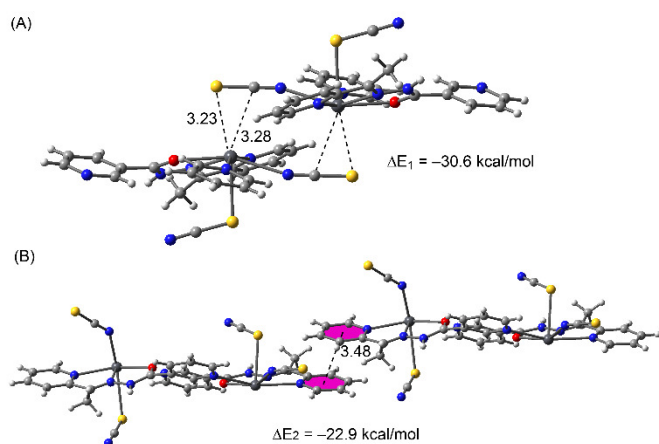


Figure 13. Theoretical models used to analyse the tetrel bonding interactions in compound **3**. Distances in Å.

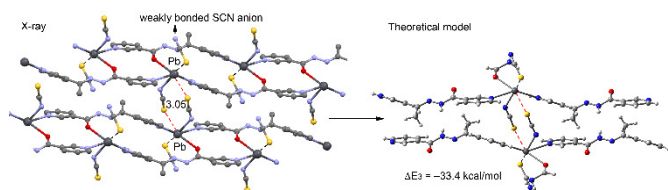


Figure 14. Left: Partial view of the X-ray structure of compound **6**. Right: Theoretical model used to analyse the tetrel bonding interactions in compound **6**. Distances in Å.

In compound **3** we have studied energetically the formation of a self-assembled dimer in the solid state that is characterized by a double tetrel bond interaction where the Pb atoms act as acceptor and the π -system of the SCN ligands as donors (Figure 13). The Pb is almost equidistant to the S and C atoms and the interaction energy is $\Delta E_1 = -30.6$ kcal/mol, indicating that each tetrel bond is approximately -15.3 kcal/mol (similar to a strong H-bond interaction). The interaction of Pb with the π -system is favoured with respect to the S-end since the electrostatic potential is anisotropic around S atom being less negative in the prolongation of the S-C bond. We have also computed the interaction energy of the antiparallel stacking between the pyridine rings observed in the solid state. This interaction is responsible for the formation of an infinite 1D chain in the crystal structure. The interaction energy is larger than expected ($\Delta E_2 = -22.9$ kcal/mol) for a stacking interaction due to the strong influence of the metal coordination to the N atom of pyridine, that reinforces the π -stacking (by increasing the dipole-dipole contribution to the interaction).

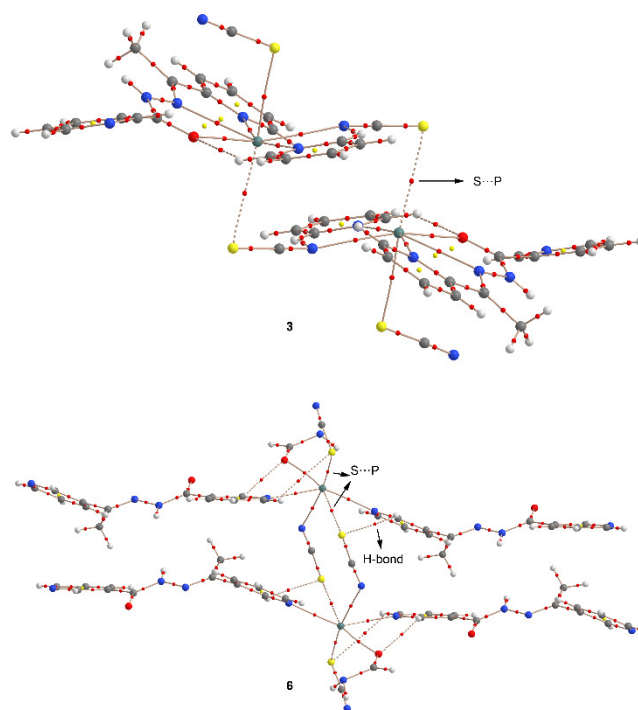


Figure 15. AIM distribution of bond and ring critical points (red and yellow spheres, respectively) in compounds **3** and **6**. The bond paths connecting bond critical points are also shown.

In compound **6**, $\text{S}\cdots\text{Pb}$ noncovalent interactions are also observed in the solid state. These interactions connect the polymeric chains that are observed in the crystal packing (see Figures 6 and 14). We have used a discrete model of the polymeric chain in order to evaluate the tetrel bonding interactions. The interaction energy of the model is $\Delta E_3 = -33.4$ kcal/mol, indicating that each tetrel bond is approximately -16.7 kcal/mol. This energy is slightly higher than the one observed for compound **3**, in good agreement with the MEP

value observed in the σ -hole, which is greater in compound **6** (see Figure 12).

Finally, we have used the Bader's theory of "atoms in molecules" (AIM) to analyse the noncovalent interactions described above. The presence of a bond critical point and a bond path connecting two atoms is a clear indication of bonding. The AIM analysis obtained for compounds **3** and **6** is shown in Figure AF4. Both tetrel bonding interactions are characterized by the presence of a bond critical point (red sphere) than connects the S atom to the Pb metal centre. In compound **6**, the S atom also interacts with a hydrogen atom of the pyridine ring since a bond critical point and bond path connecting both atoms are observed in the AIM analysis. This C–H...S hydrogen bond also contributes to the interaction between the infinite polymeric chains of the crystal structure. The values of the Laplacian of the charge density measured at the bond critical points that characterize the tetrel bonding interactions are positive, as is common in closed-shell interactions.

Conclusions

In the present study, we synthesized and fully characterised a new series of lead(II) coordination compounds assembled from the neutral nicotinoylhydrazone blocks L1 or L2 and different inorganic anions (chloride, nitrate, or thiocyanate) as auxiliary ligands. The obtained compounds range from a discrete 0D lead(II) dimer **3** and infinite 1D coordination polymers **2** and **6** to 2D metal-organic networks **1**, **4**, and **5**. Their structures are further extended via different supramolecular interactions.

In the crystal structures of **1-3**, the L1 block acts as a neutral ligand in the expected 3+1 manner, with three atoms (hydrazone oxygen and nitrogen and the 2-pyridyl nitrogen) chelating to one lead(II) cation, and one atom, the 3-pyridyl nitrogen, bridging to a neighbouring one. Unlike L1, L2 does not act as a chelating ligand, but rather behaves as a spacer between three lead(II) centres. Consequently, compounds **4-6** are all coordination polymers.

Topological classification of metal-organic (in **1**, **2**, **4**, **5** and **6**) and supramolecular (in **3**) underlying networks was performed, disclosing a uninodal 4-connected layer with the **hcb** topology in **1**, a uninodal 2-connected chain with the **2C1** topology in **2**, binodal 3,4-connected nets with the **3,4L83** topology in **3** and **4**, a 3,5-connected layer with the **gek1** topology in **5**, as well as a uninodal 3-connected chain with the **SP 1-periodic net** (4,4)(0,2) topology in **6**. Unlike the geometry and the topology of the coordination networks, the supramolecular bonding was found to be primarily defined not by the choice of the organic ligand but rather the anionic co-ligand. Interesting similarities within the pairs **1** and **4** (chloride derivatives), **2** and **5** (nitrate derivatives), and **3** and **6** (thiocyanate derivatives) were observed. The supramolecular structures of the latter compounds were found to be greatly affected by the tetrel bonding between the lead(II) containing cations and the thiocyanate moieties. These noncovalent interactions were energetically evaluated and confirmed by means of the AIM analysis.

Acknowledgements

We are grateful to the University of Maragheh for the financial support of this research. A.B. and A.F. thank DGICYT of Spain (projects CTQ2014-57393-C2-1-P and CONSOLIDER INGENIO CSD2010-00065, FEDER funds) for funding. We thank the CTI (UIB) for free allocation of computer time. AMK acknowledges the FCT (UID/QUI/00100/2013).

Notes and references

- J. C. Bailar Jr., *Prep. Inorg. React.*, 1964, **1**, 1.
- B. F. Hoskins and R. Robson, *J. Am. Chem. Soc.*, 1989, **111**, 5962.
- B. F. Hoskins and R. Robson, *J. Am. Chem. Soc.*, 1990, **112**, 1546.
- B. Moulton and M. J. Zaworotko, *Chem. Rev.*, 2001, **101**, 1629.
- A. Y. Robin and K. M. Fromm, *Coord. Chem. Rev.*, 2006, **250**, 2127.
- N. Stock and S. Biswas, *Chem. Rev.*, 2012, **112**, 933.
- K. Otsubo, Y. Wakabayashi, J. Ohara, S. Yamamoto, H. Matsuzaki, H. Okamoto, K. Nitta, T. Uruga and H. Kitagawa, *Nat. Mater.*, 2011, **10**, 291.
- S. Kitagawa, R. Kitaura and S. Noro, *Angew. Chem. Int. Ed.*, 2004, **43**, 2334.
- G. Ferey, C. Mellot-Draznieks, C. Serre, F. Millange, J. Dutour, S. Surble and Margiolaki, *Science*, 2005, **309**, 2040.
- J. R. Long and O. M. Yaghi, *Chem. Soc. Rev.*, 2009, **38**, 1213.
- H.-C.; Zhou, J. R. Long and O. M. Yaghi, *Chem. Rev.*, 2012, **112**, 673.
- Y. E. Cheon and M. P. Suh, *Angew. Chem., Int. Ed.*, 2009, **48**, 2899.
- R. Poloni, B. Smit and J. B. Neaton, *J. Am. Chem. Soc.*, 2012, **134**, 6714.
- L. J. Murray, M. Dincă and J. R. Long, *Chem. Soc. Rev.*, 2009, **38**, 1294.
- J.-R. Li, J. Sculley and H.-C. Zhou, *Chem. Rev.*, 2012, **112**, 869.
- S. Ma and H.-C. Zhou, *Chem. Commun.* 2010, **46**, 44.
- S. Yang, X. Lin, A. J. Blake, G. S. Walker, P. Hubberstey, N. R. Champness and M. Schröder, *Nat. Chem.*, 2009, **1**, 487.
- J. S. Seo, D. Whang, H. Lee, S. I. Jun, J. Oh, Y. J. Jeon and K. Kim, *Nature*, 2000, **404**, 982.
- J. Y. Lee, O. K. Farha, J. Roberts, K. A. Scheidt, S. T. Nguyen and J. T. Hupp, *Chem. Soc. Rev.*, 2009, **38**, 1450.
- L. Ma, C. Abney and W. Lin, *Chem. Soc. Rev.*, 2009, **38**, 1248.
- D. Farrusseng, S. Aguado and C. Pinel, *Angew. Chem. Int. Ed.*, 2009, **48**, 7502.
- B. Chen, S. Xiang and G. Qian, *Acc. Chem. Res.*, 2010, **43**, 1115.
- L. E. Kreno, K. Leong, O. K. Farha, M. Allendorf, R. P. Van Duyne and J. T. Hupp, *Chem. Rev.*, 2012, **112**, 1105.
- J. S. Qin, D. Y. Du, W. L. Li, J. P. Zhang, S. L. Li, Z. M. Su, X. L. Wang, Q. Xu, K. Z. Shao and Y. Q. Lan, *Chem. Sci.*, 2012, **3**, 2114.
- L. N. Dawe, T. S. M. Abedin and L. K. Thompson, *Dalton Trans.*, 2008, 1661.
- L. N. Dawe, K. V. Shuvaev and L. K. Thompson, *Inorg. Chem.*, 2009, **48**, 3323.
- L. N. Dawe, K. V. Shuvaev and L. K. Thompson, *Chem. Soc. Rev.*, 2009, **38**, 2334.
- M. Ruben, J. Rojo, F. J. Romero-Salguero, L. H. Uppadine and J.-M. Lehn, *Angew. Chem., Int. Ed.* 2004, **43**, 3644.
- M. Ruben, J.-M. Lehn and P. Müller, *Chem. Soc. Rev.*, 2006, **35**, 1056.
- V. A. Milway, S. M. T. Abedin, V. Niel, T. L. Kelly, L. N. Dawe, S. K. Dey, D. W. Thompson, D. O. Miller, M. S. Alam, P. Müller and L. K. Thompson, *Dalton Trans.*, 2006, 2835.

- 31 G. Mahmoudi, V. Stilinović, M. Servati Gargari, A. Bauzá, G. Zaragoza, W. Kaminsky, V. Lynch, D. Choquesillo-Lazarte, K. Sivakumar, A. Akbar Khandar and A. Frontera, *CrystEngComm*, 2015, **17**, 3493.
- 32 X.-P. Li, J.-Y. Zhang, M. Pan, S.-R. Zheng, Y. Liu and C.-Y. Su, *Inorg. Chem.*, 2007, **46**, 4617.
- 33 M. Yaghi, H. Li and T. L. Groy, *Inorg. Chem.*, 1997, **36**, 4292.
- 34 C.-L. Chen, B.-S. Kang and C.-Y. Su, *Aust. J. Chem.*, 2006, **59**, 3.
- 35 B. D. Wagner, G. J. McManus, B. Moulton and M. J. Zaworotko, *Chem. Commun.*, 2002, 2176.
- 36 M. Beatty, *Coord. Chem. Rev.*, 2003, **246**, 131.
- 37 M. Servati-Gargari, G. Mahmoudi, S. R. Batten, V. Stilinović, D. Butler, L. Beauvais, W. S. Kassel, W. G. Dougherty and D. VanDerveer, *Cryst. Growth Des.*, 2015, **15**, 1336.
- 38 D. S. Li, Y. P. Wu, P. Zhang, M. Du, J. Zhao, C. P. Li and Y. Y. Wang, *Cryst. Growth Des.*, 2010, **10**, 2037.
- 39 X. L. Wang, Y. Q. Chen, Q. Gao, H. Y. Lin, G. C. Liu, J. X. Zhang and A. X. Tian, *Cryst. Growth Des.*, 2010, **10**, 2174.
- 40 G. P. Yang, L. Hou, Y. Y. Wang, Y. N. Zhang, Q. Z. Shi and S. R. Batten, *Cryst. Growth Des.*, 2011, **11**, 936.
- 41 Z. Y. Du, H. B. Xu, X. L. Li and J. G. Mao, *Eur. J. Inorg. Chem.*, 2007, 4520.
- 42 B. Ding, Y. Y. Liu, X. X. Wu, X. J. Zhao, G. X. Du, E. C. Yang and X. G. Wang, *Cryst. Growth Des.*, 2009, **9**, 4176.
- 43 J. Yang, J. F. Ma, Y. Y. Liu, J. C. Ma and S. R. Batten, *Cryst. Growth Des.*, 2009, **9**, 1894.
- 44 S. H. Li, S. K. Gao, S. X. Liu and Y. N. Guo, *Cryst. Growth Des.*, 2010, **10**, 495.
- 45 T. F. Liu, J. Lu, C. B. Tian, M. N. Cao, Z. J. Lin and R. Cao, *Inorg. Chem.*, 2011, **50**, 2264.
- 46 Thirumurugan, R. A. Sanguramath and C. N. R. Rao, *Inorg. Chem.*, 2008, **47**, 823.
- 47 L. Zhang, Z. J. Li, Q. P. Lin, Y. Y. Qin, J. Zhang, P. X. Yin, J. K. Cheng and Y. G. Yao, *Inorg. Chem.*, 2009, **48**, 6517.
- 48 J. D. Lin, S. T. Wu, Z. H. Li and S. W. Du, *CrystEngComm*, 2010, **12**, 4252.
- 49 E. C. Yang, J. Li, B. Ding, Q. Q. Liang, X. G. Wang and X. J. Zhao, *CrystEngComm*, 2008, **10**, 158. 11.
- 50 J. Yang, G. D. Li, J. J. Cao, Q. Yue, G. H. Li and J. S. Chen, *Chem.–Eur. J.*, 2007, **13**, 3248.
- 51 K. L. Huang, X. Liu, J. K. Li, Y. W. Ding, X. Chen, M. X. Zhang, X. B. Xu and X. J. Song, *Cryst. Growth Des.*, 2010, **10**, 1508.
- 52 Y. H. Zhao, H. B. Xu, Y. M. Fu, K. Z. Shao, S. Y. Yang, Z. M. Su, X. R. Hao, D. X. Zhu and E. B. Wang, *Cryst. Growth Des.*, 2008, **8**, 3566.
- 53 K. Kavallieratos, J. M. Rosenberg and J. C. Bryan, *Inorg. Chem.*, 2005, **44**, 2573.
- 54 X. R. Meng, Y. L. Song, H. W. Hou, Y. T. Fan, G. Li and Y. Zhu, *Inorg. Chem.*, 2003, **42**, 1306.
- 55 R. L. Davidovicha, V. Stavilab, D. V. Marinina, E. I. Voita and K. H. Whitmire, *Coord. Chem. Rev.*, 2009, **253**, 1316.
- 56 K. L. Zhang, Y. Chang, C. T. Hou, G. W. Diao, R. T. Wu and S. W. Ng, *CrystEngComm*, 2010, **12**, 1194.
- 57 J. Yang, J. F. Ma, Y. Y. Liu, J. C. Ma and S. R. Batten, *Inorg. Chem.*, 2007, **46**, 6542.
- 58 C. Gabriel, C. P. Raptopoulou, V. Psycharis, A. Terzis, M. Zevou, C. Mateescu and A. Salifoglou, *Cryst. Growth Des.*, 2011, **11**, 382.
- 59 R. L. Davidovicha, V. Stavilab and K. H. Whitmire, *Coord. Chem. Rev.*, 2010, **254**, 2193.
- 60 M. Servati Gargari, V. Stilinović, A. Bauzá, A. Frontera, P. McArdle, D. Van Derveer, S. W. Ng and G. Mahmoudi, *Chem. Eur. J.*, 2015, 17951.
- 61 A. Bauzá, T. J. Mooibroek and A. Frontera, *Angew. Chem., Int. Ed.*, 2013, **52**, 12317.
- 62 S. J. Grabowski, *Phys. Chem. Chem. Phys.*, 2014, **16**, 1824.
- 63 (a) A. Bauzá, T. J. Mooibroek and A. Frontera, *Chem. – Eur. J.*, 2014, **20**, 10245. (b) A. Bauzá, T. J. Mooibroek and A. Frontera, *Chem. Commun.*, 2014, **50**, 12626.
- 64 J. S. Murray, P. Lane and P. Politzer, *J. Mol. Model.*, 2009, **15**, 723.
- 65 A. Bundhun, P. Ramasami, J. S. Murray and P. Politzer, *J. Mol. Model.*, 2013, **19**, 2739.
- 66 L. Shimoni-Livny, J. P. Glusker and C. W. Bock, *Inorg. Chem.*, 1998, **37**, 1853.
- 67 R. L. Davidovich, V. Stavila, D. V. Marinin, E. I. Voit and K. H. Whitmire, *Coord. Chem. Rev.*, 2009, **253**, 1316.
- 68 Oxford Diffraction (2003), *CrysAlis CCD and CrysAlis RED. Version 1.170.*, Oxford Diffraction Ltd, Wroclaw, Poland.
- 69 APEX II, v. 2011.4; Bruker AXS: Madison, WI, 2009.
- 70 SAINT+, v. 7.68A: Data Reduction and Correction Program; Bruker AXS: Madison, WI, 2009.
- 71 SADABS, v. 2008/1: An Empirical Absorption Correction Program; Bruker AXS Inc.: Madison, WI, 2008.
- 72 G. M. Sheldrick, *Acta Crystallogr.* 2008, **A64**, 112.
- 73 (a) V. A. Blatov, *IUCr CompComm Newsletter* 2006, **7**, 4; (b) V. A. Blatov, A. P. Shevchenko and D. M. Proserpio, *Cryst. Growth Des.* 2014, **14**, 3576.
- 74 (a) M. O’Keeffe and O. M. Yaghi, *Chem. Rev.* 2012, **112**, 675. (b) M. Li, D. Li, M. O’Keeffe and O. M. Yaghi, *Chem. Rev.* 2014, **114**, 1343.
- 75 R. Ahlrichs, M. Bär, M. Haser, H. Horn and C. Kölmel, *Chem. Phys. Lett.*, 1989, **162**, 165.
- 76 S. F. Boys and F. Bernardi, *Mol. Phys.* 1970, **19**, 553.
- 77 R. F. W. Bader, *Chem. Rev.* 1991, **91**, 893.
- 78 T. A. Keith, *AIMAll (Version 13.11.04)*, TK Gristmill Software, Overland Park KS, USA 2013.
- 79 M. J. Białek, J. K. Zaręba, J. Janczak and J. Zoń, *Cryst. Growth Des.*, 2013, **13**, 4039.
- 80 J. K. Zaręba, M. J. Białek, J. Janczak, J. Zon and A. Dobosz, *Cryst. Growth Des.*, 2014, **14**, 6143.
- 81 J. J. McKinnon, M. A. Spackman and A. S. Mitchell, *Acta Crystallogr.*, 2004, **B60**, 627.
- 82 S. K. Wolff, D. J. Grimwood, J. J. McKinnon, M. J. Turner, D. Jayatilaka and M. A. Spackman, *Crystal Explorer ver. 3.1*, University of Western Australia, Perth, Australia, 2013.

